**Jurnal Penelitian Fisika dan Aplikasinya (JPFA)**
*Volume 13, Issue 01, June 2023*
https://journal.unesa.ac.id/index.php/jpfa/

p-ISSN: 2087-9946
e-ISSN: 2477-1775

# Cold Surge Effect on Vertical Profile Atmosphere over Meteorological Station of Ranai Natuna: Case Study Asian Winter Monsoon 2019/2020

**Yosafat Donni Haryanto [1,a,*], Suwignyo Prasetyo [2,b], Ulil Hidayat [3,c], Wahyu Kurniawan [4,d], and Nelly Florida Riama [5,e]**

[1] Department of Meteorology, Indonesian State College of Meteorology Climatology and Geophysics, Jalan Perhubungan I No. 5, Tangerang Selatan 15221, Indonesia
[2] Center for Marine Meteorology, Indonesian Agency for Meteorology, Climatology, and Geophysics, Jalan Angkasa I, Jakarta 10610, Indonesia
[3] Kalimarau Meteorological Station, Indonesian Agency for Meteorology, Climatology, and Geophysics, Jalan Bandara Kalimarau, Berau 77315, Indonesia
[4] Center for Aeronautical Meteorology, Indonesian Agency for Meteorology, Climatology, and Geophysics, Jalan Angkasa I, Jakarta 10610, Indonesia
[5] Center for Education and Training, Indonesian Agency for Meteorology, Climatology, and Geophysics, Jalan Angkasa I, Jakarta 10610, Indonesia

e-mail: [a] yosafatdonni@gmail.com , [b] prasetyosuwignyo8@gmail.com, [c] ulil.hidayat@bmkg.go.id, [d] kurniawan.wahyu@bmkg.go.id, and [e] nelly.florida@bmkg.go.id
* Corresponding Author

*Received: 20 March 2023; Revised: 2 June 2023; Accepted: 13 June 2023*

***Abstract***

*During the Asian Winter season, which spans from November to February, the phenomenon of cold surge often occurs, leading to increased convective activity over the western Indonesian Maritime Continent. The location of Natuna Island, situated in the southern part of the South China Sea, is of particular importance for studying cold surges due to their propagation over this area. In this study, the vertical structure of the atmosphere was analyzed using radiosonde observation data collected at the Meteorological Station of Ranai Natuna. The analysis focused on physical parameters such as air temperature and relative humidity, atmospheric kinematics including wind direction and speed, as well as atmospheric thermodynamic parameters such as Lifting Condensation Level (LCL), Level of Free Convection (LFC), Equilibrium Level (EL), Convective Available Potential Energy (CAPE), and Convective Inhibition (CIN). The results indicate that during the passage of a cold surge, air temperature (T) tends to be higher in the lower troposphere, including at the surface, but lower in the middle and upper troposphere. Relative humidity (RH) also tends to be higher during cold surges, with a significant increase in the middle and upper troposphere. In the lower troposphere, the wind direction shifts from east to northeast at a higher speed compared to when a cold surge is absent. Furthermore, the LCL and LFC heights are elevated during the presence of a cold surge, while the EL height shows an insignificant decrease. It is worth noting that intense rainfall occurs, particularly when the cold surge is more pronounced, even though the values of CAPE and CIN do not change significantly.*

**Keywords:** *cold surge, physical atmosphere, kinematic atmosphere, thermodynamic atmosphere.*

**How to cite:** Haryanto Y D, et al. Cold Surge Effect on Vertical Profile Atmosphere over Meteorological Station of Ranai Natuna: Case Study Asian Winter Monsoon 2019/2020. *Jurnal Penelitian Fisika dan Aplikasinya (JPFA)*. 2023; **13**(1): 25-37.



DOI: 10.26740/jpfa.v13n1.p25-37

## INTRODUCTION

The East Asian Winter Monsoon (EAWM) is a meteorological phenomenon that significantly influences the weather and climate patterns across the Eurasian and Asia-Pacific regions, extending from the subpolar zone to the equator [1]. It is well known that the strong EAWM has an important influence on atmospheric dynamics over the Maritime Continent around Borneo and Indonesia [2,3]. The EAWM is usually defined between November and March [3–5]. In that period, from November to February, there are frequent cold surge events. A cold surge is an event that pushes the flow of cold air masses from the Siberian highlands which, if the intensity is strong, can burst to the equator. The mechanism of the cold surge has been fully reviewed by Chang et al [3] and Chang et al [2]. Cold surges often lead to increased convection activity in the maritime continent, particularly in the western region [2,6,7].

The propagation of cold surge which causes an increase in convection activity heightens the potential for heavy rainfall. [2,7–9]. In some cases, cold surge events can also result in hydrometeorological disasters if they occur together with other phenomena, such as the Madden Julian Oscillation (MJO) and Borneo Vortex [10,11]. However, a cold surge that occurs alone can also result in a hydrometeorological disaster if atmospheric conditions, both on a local and synoptic scale, support the growth of convective clouds that cause rainfall [12,13]. In this case, cold surges that cross the equator are more prone to influence from heavy rains to hydrometeorological disasters in the southern and western regions of Indonesia [14]. One example is when a cold surge together with other phenomena such as MJO and equatorial waves resulted in the highest extreme rainfall since 1866 which then resulted in severe flooding in early 2020 [15].

Convection activity associated with rainfall clouds is represented by the physical and kinematic profile of the atmosphere along with the thermodynamic profile of the atmosphere [16]. These profiles or parameters are obtained from radiosonde observation data to obtain their values vertically in all layers of the troposphere. One of the programs of the Years of Maritime Continent, which is still ongoing today, is to capture how cold surges behave based on observations of radiosonde aerial data [17]. To analyze the behavior of cold surges, the Intensive Observation Period involved conducting four daily observations in Jakarta and Pangkal Pinang. Upper air observations using a radiosonde were utilized for this purpose. [18]. Research conducted by Makmur et al [18] revealed that there were seven cold surges that propagated across the equator which then resulted in extreme rainfall reaching 150 mm/day. However, this study focuses on cold surges that cross the equator, while cold surges that propagate north of the equator are not included in the analysis.

The thermodynamic structure of cold surge propagation has been studied in various areas, including the South China Sea [19], in the Philippines [20-21], and the Malaysian peninsula [22]. In this context, the cold surge that propagates across the South China Sea region to the western part of the Indonesian Maritime Continent, including Natuna Island, is of particular interest. Therefore, the presence of the Ranai Natuna Meteorological Station plays a crucial role in observing the atmosphere, especially in studying cold surge propagation.

Although previous studies have described the dynamic and thermodynamic structure of the atmosphere during cold surge events, they often had limited temporal scale data [22]. It is well-known that each cold surge event possesses unique characteristics and can occur multiple times within a given year in a particular region. Hence, this study aims to enhance our understanding of these characteristics by conducting a statistical analysis of parameter data over a four-month period. Additionally, previous research locations were considered limited in comprehensively describing the cold surge characteristics in the eastern region of the Indonesian Maritime Continent. Thus, Natuna Island was selected as the study location due to

its strategic position during cold surge propagation in the Indonesian maritime continent. The study optimizes twice-daily radiosonde data collected at 00 and 12 UTC and employs boxplot analysis to address anomalies that may arise in highly variable and extreme atmospheric conditions. The expected outcome of this study is to provide a deeper understanding of atmospheric kinematics and thermodynamics during cold surge propagation in the Indonesian Maritime Continent region.

## METHOD

The data utilized in this study comprised of 850 mb layer wind data and radiosonde data. The 850 mb layer wind data were obtained from the ECMWF-ERA5 reanalysis model, with a spatial resolution of 0.25 × 0.25 and a temporal resolution of 6 hours [23]. On the other hand, radiosonde data was collected from the Ranai Natuna Meteorological Station at a temporal resolution of every 12 hours (00 and 12 UTC). The reanalysis and radiosonde data were gathered specifically during the Asian Winter period, spanning from November to February in the year 2019/2020.

The utilization of observational data for studying cold surges is considered crucial. Upper air observation data can serve as both analytical and predictive tools for detecting cold surge events, providing insights for the upcoming hours or days following the identification of a cold surge. In this context, the Ranai Natuna Meteorological Station holds a strategic position for detecting cold surge events since it lies directly along the propagation path of cold surges (Figure 1). The time period of 2019/2020 was selected as the initial study to investigate how cold surges affect the vertical atmospheric profile when propagating through the Ranai Natuna Meteorological Station.

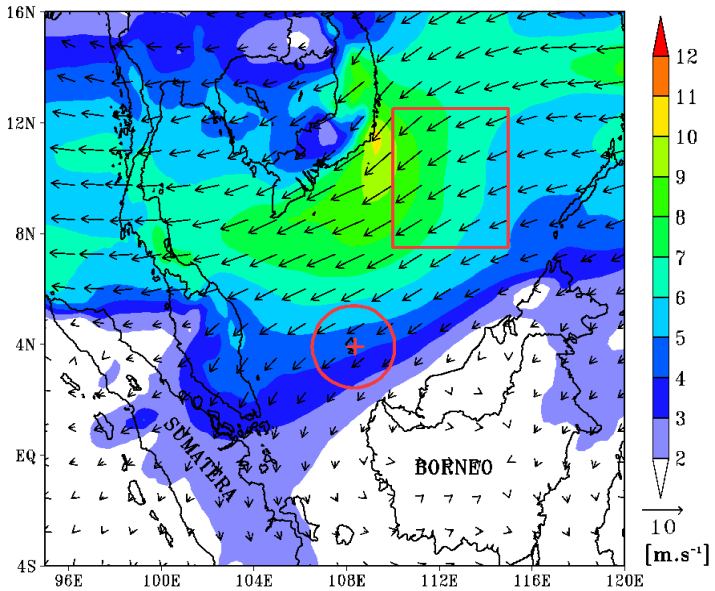


**Figure 1.** Average wind direction and speed for November - March in the 2019/2020 Asian Winter period. The cold surge index is taken from the average wind layer of 850 mb in the area inside the red box. The "+" sign represents the radiosonde observation point, while the red circle represents the ideal coverage area of the radiosonde data (radius of about 200 km in a 100 mb layer) [24].

Cold surge is identified when the average meridional wind speed of the 850 mb layer within the specified box area in Figure 1 reaches 8 m/s or higher [25]. The occurrence of a cold surge is typically initiated by the presence of a high-pressure area over the Siberian plateau and a

relatively high pressure difference between this area and the southern coast of the Chinese plains. This is followed by a significant temperature decrease and an increase in meridional wind speed in the South China Sea region [5]. The utilization of meridional winds in the South China Sea region to detect cold surges is considered reliable, as supported by several previous studies (e.g., [25–27]).

The analysis in this study focused on the vertical profile of the atmosphere, comparing days with and without cold surges based on radiosonde observation data. The parameters analyzed were divided into three categories: atmospheric physical parameters, atmospheric kinematics, and atmospheric thermodynamics. The atmospheric physical parameters included air temperature (T) and relative humidity (RH). The atmospheric kinematic parameters comprised wind direction and speed. The atmospheric thermodynamic parameters encompassed the lifting condensation level (LCL), level of free convection (LFC), equilibrium level (EL), convective available potential energy (CAPE), and convective inhibition (CIN). These parameters were obtained from https://weather.uwyo.edu/upperair/sounding.html.

For analysis convenience, days characterized by the presence or absence of cold surges are designated as CS (cold surge) and NS (no surge) respectively. Additionally, the symbols used in conducting the analysis are determined based on the temporal resolution of the radiosonde observation data.

1. CS00 : cold surge at 00 UTC
2. CS12 : cold surge at 12 UTC
3. NS00 : no surge at 00 UTC
4. NS12 : no surge at 12 UTC

## RESULTS AND DISCUSSION

### The Occurrence of Cold Surge 2019/2020

The CS phenomenon is characterized by a relatively high pressure gradient between the Siberian plateau and the south coast of China, a significant decrease in surface temperature in the Hong Kong area, to an increase in wind speed (low level) in the South China Sea [5]. Some of these indications are often used as indicators to identify the occurrence of CS as done by Adrian and Utama [28] and have been used as operational guidelines as an index of detection of CS events by the Indonesian Agency for Meteorology, Climatology, and Geophysics (BMKG) (http://web.meteo.bmkg.go.id/id/observation/index-surge). However, it is worth noting that many researchers primarily identify CS using low-layer meridional wind speeds specifically in the vicinity of the South China Sea. CS is typically considered active when it surpasses a certain threshold value (e.g., [25–27]).

Figure 2 presents the CS index, depicted as a 12-hour time series, accompanied by a daily rainfall chart spanning from November to February. Overall, CS occurred eight times with the maximum intensity occurring around December 1 to 13. A significant CS index in this period is associated with light to heavy rainfall events. The highest rainfall occurred on December 9, 2019, with a value of 95.7 mm/day. Chang and Lau [29] revealed an increase in convective activity occurred about one day after CS propagated in the South China Sea. This observation aligns with the findings of our study, which indicate that CS events contribute to rainfall characterized by varying intensities, ranging from light to heavy. These results are also consistent with the previous research conducted by Makmur et al [30].

The occurrence of CS events exhibits a higher frequency during the initial phase of the Asian Winter period, specifically in November and December. This notable frequency is evident from the CS index depicted in Figure 2, emphasizing the significance of these events during the mentioned period. This is in accordance with the findings of Xavier et al [27] which stated that

CS was more active in the first half of the season from November to February. These conditions then resulted in rainfall in most parts of the Indochina Peninsula to Malaya and the northern part of Borneo. In this instance, the inclusion of the Ranai Natuna Meteorological Station within the study area is justified based on the observed CS index and the occurrence of notably higher rainfall, particularly during the period spanning from November to early January (Figure 2).

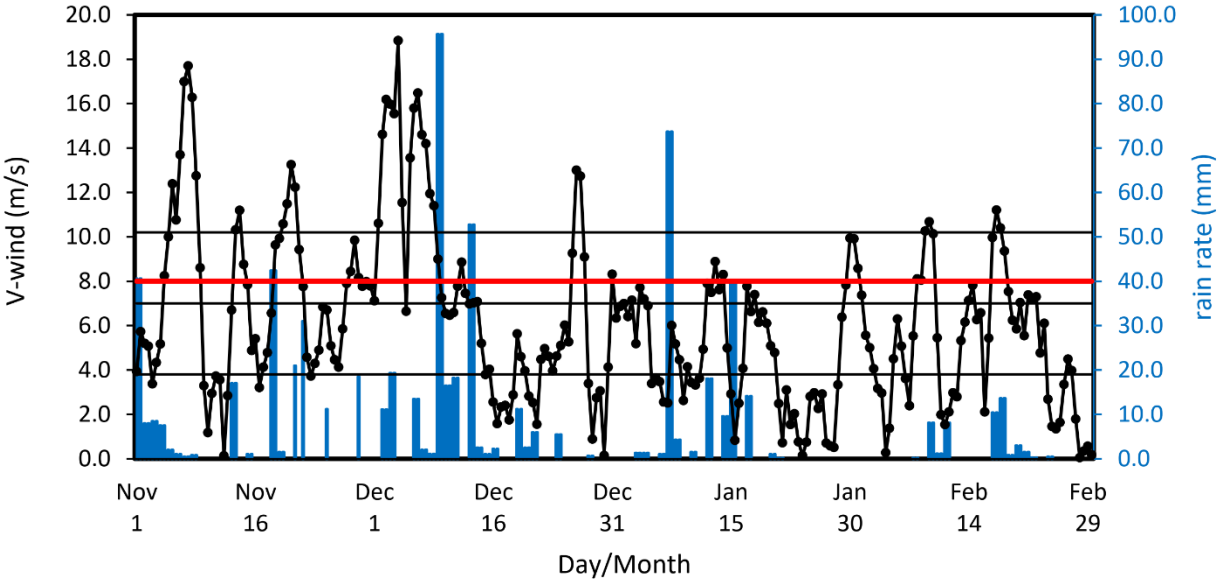


**Figure 2.** Time series of cold surge index. The red horizontal line is the threshold indicator for cold surges based on meridional wind speed (v-wind) when the value is more than 8 m/s.

**Atmospheric Physical and Kinematic Profiles**

In general, the temperature values vary greatly depending on the layer height (Figure 3.a). The higher the layer, the lower the temperature value. Based on the temporal distribution, in general, the temperature value at 12 UTC has a higher value than 00 UTC, both in the CS and NS cases. The temperature values at 12 UTC in several layers seem to fluctuate more easily, especially in the case of CS. The details of temperature parameters in each layer of the atmosphere are described in the following paragraphs.

The temperature value experienced a significant increase (decrease) in the 1000 mb layer (850 and 500 mb). Meanwhile, for other layers (surface and 200 mb) there is no significant change. The surface layer, both at 00 UTC and 12 UTC, did not experience a significant change in temperature when CS was present. However, in the 1000 mb layer, there is a significant increase in value reaching +0.8°C at 12 hours UTC. Contrarily, the 850 mb layer exhibited a decline in its median data, reaching a value of -0.5°C during the occurrence of a CS at 00 UTC and 12 UTC. In the 500 mb layer, there is (no) significant change at 12 UTC (00 UTC) with a decrease value reaching -0.4°C. Meanwhile, for the 200 mb layer, there is no significant change either at 00 or 12 UTC.

The distribution of RH data is increasingly spread out with increasing altitude (Figure 3.b). This shows that the RH values at 500 mb and 200 mb are more varied than at 850 mb. Within the surface layer and at 1000 mb, the majority of RH values fall within the range of 85% to 95%. Notably, the RH values at 00 UTC tend to be higher than those at 12 UTC. Analysis of the median values reveals no significant alteration in RH values between CS and NS cases within the surface layer and at 1000 mb. However, at 850 mb, 500 mb, and 200 mb, RH tends to be higher during CS events. This difference increases gradually as the altitude increase. At 200 mb, the difference in the median RH value reaches 8%. In addition, the RH value decreases with increasing

altitude. In this instance, the relative humidity (RH) values at 850 mb exhibit a distribution ranging from 80% to 98%. At 500 mb, the majority of values fall within the range of 55% to 95%, while at the 200 mb layer, the distribution spans from 30% to 70%.

The increasing temperature at the lower troposphere is due to air mass modification by the warm sea surface during its long propagation over the South China Sea [31-32]. This result is consistent with previous studies done by Samah, et al [22] and Ogino et al [21] that higher temperatures were observed at the surface during the passage of the CS. RH in the lower troposphere (below 1000 mb) was suspected to be impacted by the high temperature at the surface as the value is lower compared to the layer above. High temperatures at the lower troposphere also lead to the formation of shallow layer super adiabatic lapse rate during the passage of the CS over the station [22]. Despite the temperature variation was observed up to 500 mb, the CS passage mostly confined in a shallow layer between the surface and the 850 mb [33]. This contradiction could be possible as temperature variation at 500 mb is vary due to convective activity instead of horizontal advection by the propagation of the CS.

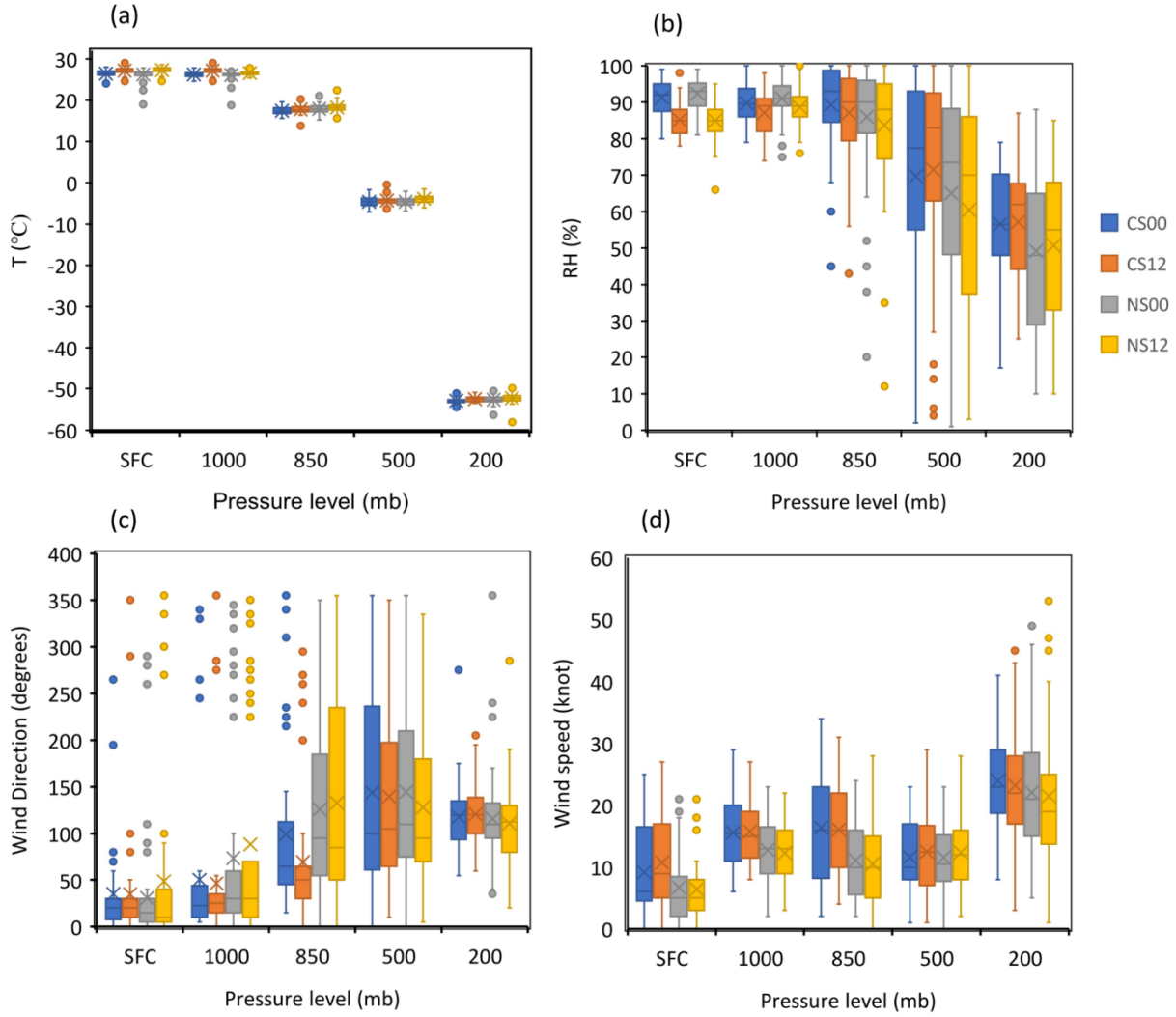


**Figure 3.** Atmospheric physical parameters for (a) temperature, (b) relative humidity, (c) wind direction, and (d) wind speed on the surface layer, 1000, 850, 500, and 200 mb (horizontal axis). CS (NS) denotes cold surge (no surge), while 00 and 12 are the hour markers in UTC.

The wind direction profile at the 850 mb layer (surface up to 1000 mb) changes significantly (insignificantly) in the case of CS (Figure 3.c). In the surface layer and 1000 mb, the distributed

wind direction is mostly in the range of 0-100 degrees, with some outsiders within 200-350 degrees range. Based on the median value, in these two layers, there is no significant difference in wind direction when CS is present and absent. At layer 850 mb, the wind direction varies more. It can be seen that when there is CS, the wind direction is distributed mostly in the range of 0 – 150 degrees, whereas when there is no CS, the values are very scattered/distributed in a wide range in all directions. The median data shows that when CS occurs, the wind direction is generally in the range of 50 – 60 degrees. Whereas when there is no CS, the median wind speed is within the 85-100 degrees range. Thus, the wind direction profile shows that there is a significant change in direction in the 850 mb layer, wherein the NS case originates from the East and subsequently transitions to the Northeast in the CS case.

The wind direction profile at 500 mb and 200 mb layers did not show a significant change in the CS case (Figure 3.c). In the 500 mb layer, this can be seen from the median values which are almost the same, namely 95 – 110 degrees (East to Southeast). The data distribution is very wide and spreads mostly in 50 – 240 degrees. The wind direction at the 200 mb layer exhibits similarities to the 500 mb layer. Based on the median value, there is no noteworthy alteration in wind direction during the occurrence of CS. The distribution of wind directions is narrower, with a majority of values falling between 80 and 130 degrees.

The wind speed profile based on its temporal distribution generally shows no significant difference for wind speeds at 00 UTC and 12 UTC in all layers (Figure 3.d). Considering the data distribution, except for the 500 mb layer, the wind speed tends to increase as the height of the atmospheric layer increases. In the surface layer, wind speed values are more distributed when there is CS, where most values are in the range of 5-16 knots and when NS the wind speed is only in the range of 2-8 knots. Based on the median value, the wind speed experienced a significant increase (reaching 5 knots) when CS occurred (Median CS00 = 6 knots, CS12 = 9 knots, NS00 = 5 knots, NS12 = 5 knots). In the 1000 mb layer, the distribution of wind speed values is similar, but with distinct ranges. During CS events, the majority of wind speeds fall within the range of 11-20 knots, whereas during the absence of CS, the range is 9-16 knots. Based on the median value, there is an increase in wind speed during CS events (reaching 3 knots) (Median CS00 = 16 knots, CS12 = 15 knots, NS00 = 13 knots, NS12 = 13 knots).

The wind speed profile at the 850 mb layer is more distributed and has a higher value when CS occurs, where the values are mostly distributed in the range of 9 – 23 knots (Figure 3.d). Whereas in the NS case, the values are mostly distributed between 6 – 16 knots. Based on the median value, the wind speed increases significantly when CS occurs (up to 6 knots) (Median CS00 = 16 knots, CS12 = 16 knots, NS00 = 10 knots, NS12 = 10 knots). In the 500 mb layer, the wind speed value is not greater than 850 mb. The wind speed distribution has almost the same value, both in the CS and NS cases, where the wind speed distribution is mostly in the range of 8-17 knots. Based on the median value, wind speed does not change significantly when CS occurs (Median CS00 = 10 knots, CS12 = 13 knots, NS00 = 11 knots, NS12 = 12 knots). In the 200 mb layer, wind speed has a wide data distribution with a higher range of values compared to the other layers. In the CS (NS) case, wind speeds are distributed mostly in the range of 17-29 knots (15-28 knots). Based on the median value, the wind speed has increased by 3 knots in the CS case (Median CS00 = 23 knots, CS12 = 22 knots, NS00 = 21 knots, NS12 = 19 knots).

The observed changes in wind direction and speed in this study align with findings from a previous study [22]. The presence of CS results in a shift in wind direction towards the northwest and an increase in strength with altitude. This change in wind direction in the lower layers and the strengthening of winds with height can be attributed to the passage of the CS [22]. It is worth noting that the wind speed at 500 mb did not show significant changes. This could be attributed to a greater influence of vertical movement rather than horizontal movement

in that layer. As mentioned earlier, significant changes primarily occurred in the lower and upper troposphere. This is because the passage of the CS is mainly confined to the lower troposphere below 850 mb [33]. Whereas in the upper troposphere (represented by 200 mb), wind speed also increases significantly due to the intensification of Hadley cell and enhanced upper tropospheric outflow in the tropic as the passage of CS leads to the development of deep convective clouds [29].

**Atmospheric Thermodynamic Profiles**

The LFC value at 00 UTC has a smaller distribution compared to the LFC at 12 UTC (Figure 4.a). At 00 UTC, the data is mostly distributed at 950 – 970 mb and at 12 UTC at 925 – 965 mb. On average, the LFC value is lower during the occurrence of a cold surge (CS) at both 00 UTC and 12 UTC, as indicated by the median values, compared to the the absence of CS (Median CS00 = 955 mb, CS12 = 950 mb, NS00 = 963 mb, NS12 = 960 mb). In other words, when there is a CS event, the LFC value decreases compared to the absence of CS. Even though the average value of the NS data is smaller than that of the CS data, this can be neglected considering the large number of outsider data in the NS data. Outsider data is data whose value is extreme and unusual compared to other data in the group. In the boxplot, this data is plotted in different shapes (small circles) and is above or below the ends of the fence/whisker [34]. This outsider has an extreme and unusually low value, thus making the calculation of the average LCL value in the NS data very small.

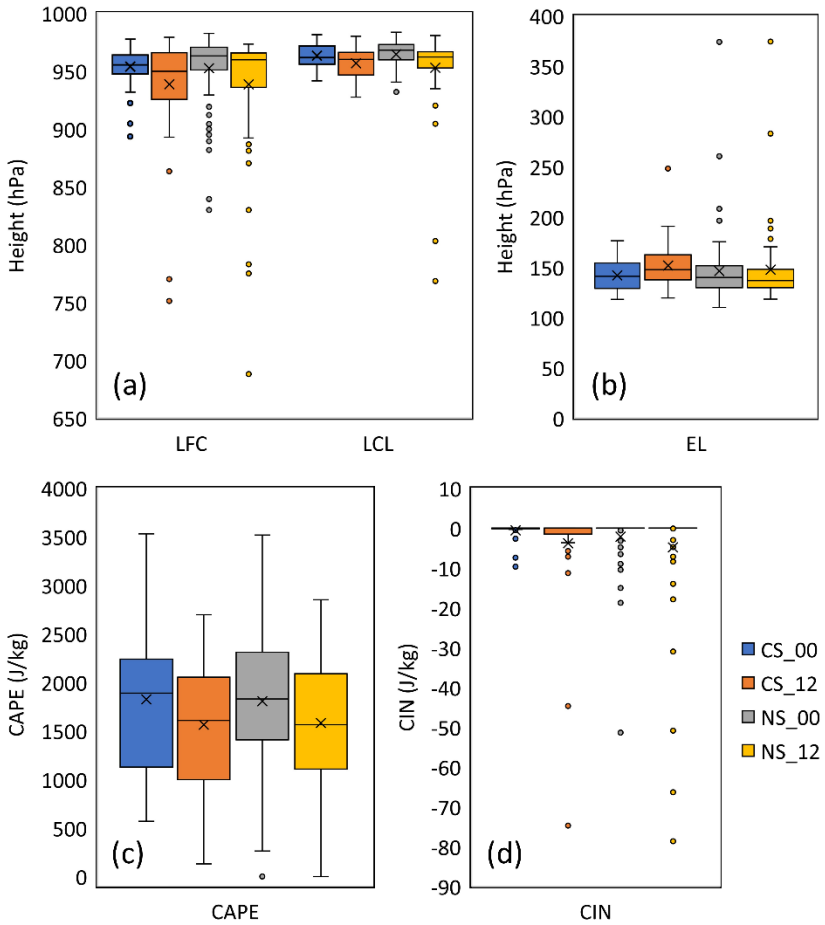


**Figure 4.** Atmospheric thermodynamic parameters (a) LCL and LFC, (b) EL, (c) CAPE, (d) CIN. CS (NS) denotes cold surge (no surge), while 00 and 12 are the hour markers in UTC.

Based on data distribution, the LCL value at 00 UTC has a smaller distribution than the LCL value at 12 UTC (Figure 4.a). Compared to data when CS is present, the LCL value in the NS case has many outsiders in the layer range of 750 – 950 mb. This means that when CS is present, LCL values tend to have a small range and there are almost no unusual extreme value data. Based on the median, in general when there is CS, both 00 and 12 UTC, the LCL value has decreased compared to the NS case (Median CS00 = 962 mb, CS12 = 960 mb, NS00 = 968 mb, NS12 = 962 mb). When there is CS at 00 UTC, the LCL values are mostly distributed in 956 – 972 mb layers, whereas when the CS is absence, LCL values are distributed at 960 – 973 mb. For 12 UTC, the LCL values are mostly distributed in layers 947 – 966 mb when CS is present and within 953 – 967 mb when CS is absence.

The EL value in the NS case has many outsiders compared to the value in the CS case (Figure 4.b). This suggests that during a CS event, the occurrence of extreme and unusual EL values is rare. In terms of data distribution, EL values during CS exhibit a wider range compared to the absence of CS. However, based on the median value, there is no significant difference in EL values between CS and non-CS conditions (Median CS00 = 141 mb, CS12 = 148 mb, NS00 = 140 mb, NS12 = 137 mb).

The distribution of CAPE values in CS cases is slightly less sparse than in NS cases (Figure 4.c). At 00 UTC, when there is CS, the CAPE value generally varies in the range 1131 – 2239 J/Kg and the value varies in the range 1428 – 2307 J/Kg when the CS is absence. Whereas at 12 UTC, when there is CS the CAPE values vary in the range 1001 – 2010 J/Kg and in the range of 1242 – 2089 J/Kg when the CS is absence. Based on the median value, compared to the absence of CS, the CAPE value when CS is present is slightly higher but not significant (Median CS00 = 1889 J/Kg, CS12 = 1606 J/Kg, NS00 = 1847 J/Kg, NS12 = 1591 J/Kg ). Thus, the CAPE value does not change significantly when there is CS compared to when there is no CS.

The distribution of CIN values in general, both in the presence and absence of CS, is very large. Most of the value is 0 and sometimes in some cases, the value drops significantly to -80 J/Kg. This makes the boxplot difficult to interpret. There is a lot of outsider event data which makes the calculation of the average CIN value less representative. So that the CIN value in this case is less affected or there is no significant difference when there is CS compared to the absence of CS.

It is important to note that the term decreased (increased) in previous analysis indicates that the height of LCL, LFC, or EL was elevated (reduced). In this situation, the overall decrease of LCL when there is CS was caused by insufficient moisture content in the lower troposphere, as this is also found in the previous study [22]. As mentioned in the previous analysis, insignificant changes in moisture content in the lower troposphere were related to the increase in temperature. Since LCL is the first level at which saturation is attained as an air parcel lifted from the surface, when LCL is elevated, this is due to insufficient moisture at the surface in case of non-occurrence of rainfall [22]. The same profile of LCL has occurred to LFC, that is the height of LFC was elevated when there is a CS event. On the other side, the height of EL was much lower when CS is present compared when CS is absence. These conditions indicate that the depth of the unstable layer is shallower when CS is present [22].

As the thermodynamic structure of the atmosphere is needed for analysis of convection activity, CAPE and CIN are the two common indices that important enough in such analysis. CAPE quantifies the amount of energy contained within an atmospheric gas parcel, which is essential for the formation of convective clouds. Meanwhile, CIN measures the amount of energy that inhibits the development of a convective cloud within a parcel. As previously discussed, the study findings indicate that the values of CAPE and CIN do not show significant changes in the presence of CS compared to its absence. The overall value of CAPE and CIN is

favorable to the development of convective clouds, whether CS is present or not. However, although the thermodynamic structure was favorable for the surface air parcel to attain LFC, the surface air parcel was unable to rise further on its own in the absence of local heating (instability mechanism). Hence, the thermodynamic structure was not favorable for triggering local convection during the passage of the CS [22].

This study still has limitations in the temporal resolution of radiosonde observations that were only carried out during the morning (00 UTC) and afternoon (12 UTC). Thus, the effect of the CS on convective cloud formation is less represented using only radiosonde data. Convective cloud formation in Indonesia predominantly takes place during daylight hours, with solar radiation playing a crucial role in driving the evaporation process. Apart from the constraints related to data density, the assessment of atmospheric stability in this study was restricted to the utilization of the CAPE and CIN indices. Nevertheless, it is worth noting that several other atmospheric stability indices exist, which could potentially offer valuable insights into the determination of convective activity levels. This research is the first step to determine the influence of CS when it spreads towards the equator. Further research can develop by utilizing radiosonde data as a supporting index in determining whether CS is active based on several parameters that can be derived from radiosonde observations.

## CONCLUSION

The occurrence of a cold surge, as represented by the meridional wind index, resulted in rainfall in the Ranai Natuna Meteorological Station area. Cold surges lead to higher air temperatures in the lower troposphere, including at the surface, but lower temperatures in the upper and middle troposphere. The relative humidity is higher during cold surges, with a significant increase in the upper troposphere. In addition, in the lower troposphere, the wind direction changes from east to northeast at a higher speed compared to when a cold surge is absent. The lifting condensation level (LCL) and level of free convection (LFC) were elevated when a cold surge was present, while the height of the equilibrium level (EL) decreased, although not significantly. On the other hand, the values of convective available potential energy (CAPE) and convective inhibition (CIN) generally remained unchanged during the occurrence of a cold surge. Nevertheless, the value of CAPE, which serves as the main indicator of the potential for convective cloud formation, remains significant in supporting the growth of convective clouds that cause rainfall.

## ACKNOWLEDGMENT

The authors (YDH, SP, UH, WK) would like to acknowledge Center for Education and Training from Indonesian Agency for Meteorology, Climatology, and Geophysics for funding acquisition to this research.

## AUTHOR CONTRIBUTIONS

Yosafat Donni Haryanto: Conceptualization and Supervision; Suwignyo Prasetyo: Conceptualization, Methodology, Formal Analysis, Writing - Original Draft, Writing - Review & Editing, Visualization; Ulil Hidayat: Formal Analysis, Data Curation, Writing - Review & Editing; Wahyu Kurniawan: Formal Analysis, Writing - Review & Editing; Nelly Florida Riama: Funding acquisition.

## DECLARATION OF COMPETING INTEREST

The authors declare that they have no known competing financial interests or personal relationships that could have appeared to influence the work reported in this paper.

**REFERENCES**


[1] Huang R, Chen J, Wang L, and Lin Z. Characteristics, Processes, and Causes of the Spatio-Temporal Variabilities of the East Asian Monsoon System. *Advances in Atmospheric Sciences*. 2012; **29**(5): 910–942. DOI: https://doi.org/10.1007/s00376-012-2015-x.

[2] Chang C-P, Lu M-M, and Lim H. Monsoon Convection in the Maritime Continent: Interaction of Large-Scale Motion and Complex Terrain. *Meteorological Monographs*. 2016; **56**: 6.1-6.29. DOI: https://doi.org/10.1175/amsmonographs-d-15-0011.1.

[3] Chang C-P, Wang Z, and Hendon H. *The Asian Winter Monsoon*, in: B. Wang (Ed.), The Asian Monsoon. New York: Springer Berlin Heidelberg; 2006: pp. 89–127. DOI: https://doi.org/10.1007/3-540-37722-0_3.

[4] Ding Y. *The Winter Monsoon in East Asia*, in: D. Yihui (Ed.), Monsoons Over China. Dordrecht: Springer Netherlands; 1994: pp. 91–173. DOI: https://doi.org/10.1007/978-94-015-8302-2_2.

[5] Chan JLC and Li C. *The East Asia Winter Monsoon*, in: C.-P. Chang (Ed.), East Asian Monsoon. New Jersey: World Scientific Publishing Co. Pte. Ltd.; 2004: pp. 54–106. DOI: https://doi.org/10.1142/9789812701411_0002.

[6] Wijayanti VA, Hidayat R, Faqih A, and Alfahmi F. The Impact of the Interaction Between Madden-Julian Oscillation and Cold Surge on Rainfall over Western Indonesia. *Indonesian Journal of Geography*. 2021; **53**(2): 245–253. DOI: http://dx.doi.org/10.22146/ijg.64006.

[7] Abdillah MR, Kanno Y, Iwasaki T, and Matsumoto J. Cold Surge Pathways in East Asia and Their Tropical Impacts. *Journal of Climate*. 2021; **34**(1): 157–170. DOI: https://doi.org/10.1175/JCLI-D-20-0552.1.

[8] Lim SY, et al. Impacts of Boreal Winter Monsoon Cold Surges and the Interaction with MJO on Southeast Asia Rainfall. *Journal of Climate*. 2017; **30**(11): 4267–4281. DOI: https://doi.org/10.1175/JCLI-D-16-0546.1.

[9] Tan I, et al. Wet and Dry Cold Surges Over the Maritime Continent. *ESS Open Archive*. 2022; preprint. DOI: https://doi.org/10.1002/essoar.10512941.1.

[10] Tangang FT, et al. On the Roles of the Northeast Cold Surge, the Borneo Vortex, the Madden-Julian Oscillation, and the Indian Ocean Dipole During the Extreme 2006/2007 Flood in Southern Peninsular Malaysia. *Geophysical Research Letters*. 2008; **35**(14): L14S07. DOI: https://doi.org/10.1029/2008GL033429.

[11] Purwaningsih A, Tank AK, and Vila J. Atmospheric Conditions Associated with Northerly Surge, Borneo Vortex and Madden Julian Oscillation During the Extreme Rainfall Cases in Early 2021 Over the Western Part of the Maritime Continent. *Springer Proceedings in Physics*. 2022; **275**: 717–735. DOI: https://doi.org/10.1007/978-981-19-0308-3_57.

[12] Wu P, et al. The Impact of Trans-Equatorial Monsoon Flow on the Formation of Repeated Torrential Rains over Java Island. *Scientific Online Letters on the Atmosphere*. 2007; **3**: 93–96. DOI: https://doi.org/10.2151/sola.2007-024.

[13] Nuryanto DE, Pawitan H, Hidayat R, and Aldrian E. Characteristics of Two Mesoscale Convective Systems (MCSs) over the Greater Jakarta: Case of Heavy Rainfall Period 15–18 January 2013. *Geoscience Letters*. 2019; **6**(1): 1. DOI: https://doi.org/10.1186/s40562-019-0131-5.

[14] Hattori M, Mori S, and Matsumoto J. The Cross-Equatorial Northerly Surge Over the Maritime Continent and Its Relationship to Precipitation Patterns. *Journal of the Meteorological Society of Japan. Ser. II*. 2011; **89A**: 27–47. DOI: https://doi.org/10.2151/jmsj.2011-A02.

[15] Lubis SW, et al. Record-Breaking Precipitation in Indonesia's Capital of Jakarta in Early January 2020 Linked to the Northerly Surge, Equatorial Waves, and MJO. *Geophysical*

*Research Letters*. 2022; **49**(22): e2022GL101513. DOI: https://doi.org/10.1029/2022GL101513.
[16] Nuryanto DE, Pawitan H, Hidayat R and Aldrian E. Kinematic and Thermodynamic Structures of Mesoscale Convective Systems During Heavy Rainfall in Greater Jakarta. *Makara Journal of Science*. 2018; **22**(3): 127–136. DOI: https://doi.org/10.7454/mss.v22i3.8291.
[17] Yoneyama K and Zhang C. Years of the Maritime Continent. *Geophysical Research Letters*. 2020; **47**(12): e2020GL087182. DOI: https://doi.org/10.1029/2020GL087182.
[18] Makmur E, et al. Characteristics of 7 Northerly Cold Surge Events During Years of the Maritime Continent Campaign 2021. *EGU General Assembly 2022*. 2002; EGU22-2111. DOI: https://doi.org/10.5194/egusphere-egu22-2111.
[19] Hattori M, et al. The Impact of Additional Radiosonde Observations on the Analysis of Disturbances in the South China Sea during VPREX2010. *Scientific Online Letters on the Atmosphere*. 2016; **12**(1): 75–79. DOI: https://doi.org/10.2151/sola.2016-018.
[20] Hattori M, et al. Impact of the Radiosonde Observations of Cold Surge Over the Philippine Sea on the Tropical Region and the Southern Hemisphere in December 2012. *Sola*. 2017; **13**: 19–24. DOI: https://doi.org/10.2151/sola.2017-004.
[21] Ogino S, et al. Cold Surge Event Observed by Radiosonde Observation from the Research Vessel "Hakuho-Maru" Over the Philippine Sea in December 2012. *Progress in Earth and Planetary Science*. 2018; **5**: 9. DOI: https://doi.org/10.1186/s40645-017-0163-4.
[22] Samah AA, et al. Thermodynamic and Dynamic Structure of Atmosphere Over the East Coast of Peninsular Malaysia During the Passage of a Cold Surge. *Journal of Atmospheric and Solar-Terrestrial Physics*. 2016; **146**: 58–68. DOI: https://doi.org/10.1016/j.jastp.2016.05.011.
[23] Hersbach H, et al. The ERA5 Global Reanalysis. *Quaterly Journal of the Royal Meteorological Society*. 2020; **146**(730): 1999–2049. DOI: https://doi.org/10.1002/qj.3803.
[24] Wirjohamidjojo S and Swarinoto Y. *Synoptic Meteorology (Analysis and Assessment of Synoptic Weather Analysis Results)*. Center for Research and Development, BMKG; 2013.
[25] Koseki S, Koh TY, and Teo CK. Borneo Vortex and Mesoscale Convective Rainfall. *Atmospheric Chemistry and Physics*. 2014; **14**(9): 4539–4562. DOI: https://doi.org/10.5194/acp-14-4539-2014.
[26] Chang C-P, Harr PA, and Chen HJ. Synoptic Disturbances Over the Equatorial South China Sea and Western Maritime Continent During Boreal Winter. *Monthly Weather Review*. 2005; **133**(3): 489–503. DOI: https://doi.org/10.1175/MWR-2868.1.
[27] Xavier P, et al. Seasonal Dependence of Cold Surges and Their Interaction with the Madden–Julian Oscillation Over Southeast Asia. *Journal of Climate*. 2020; **33**(6): 2467–2482. DOI: https://doi.org/10.1175/JCLI-D-19-0048.1.
[28] Aldrian E and Utama GSA. Identifikasi dan Karakteristik Seruak Dingin (Cold Surge) Tahun 1995-2003. *Jurnal Sains Dirgantara*. 2007; **4**(2): 107–127. Available from: https://jurnal.lapan.go.id/index.php/jurnal_sains/article/view/667.
[29] Chang C-P and Lau KM. Short-Term Planetary-Scale Interactions Over the Tropics and Midlatitudes During Northern Winter. Part I: Contrasts Between Active and Inactive Periods. *Monthly Weather Review*. 1982; **110**(8): 933–946. DOI: https://doi.org/10.1175/1520-0493(1982)110<0933:STPSIO>2.0.CO;2.
[30] Makmur E, et al. An Overview of Cold Surge Observation During 2021 Years of the Maritime Continent Campaign. *AGU Fall Meeting Abstract*. 2021: pp. A53C-03. Available from: https://ui.adsabs.harvard.edu/abs/2021AGUFM.A53C..03M/abstract
[31] Chang C-P, Erickson JE and Lau KM. Northeasterly Cold Surges and Near-Equatorial Disturbances over the Winter MONEX Area During December 1974. Part I: Synoptic Aspects. *Monthly Weather Review*. 1979; **107**: 812–829. DOI: https://doi.org/10.1175/1520-

0493(1980)108<0298:NCSANE>2.0.CO;2.

[32] Johnson RH and Zimmerman JR. Modification of the Boundary Layer Over the South China Sea During a Winter MONEX Cold Surge Event. *Monthly Weather Review*. 1986; **114**(11): 2004–2015. DOI: https://doi.org/10.1175/1520-0493(1986)114<2004:motblo>2.0.co;2.

[33] Ramage CS. *Monsoon Meteorology*. New York: Academic Press; 1971.

[34] Wilks D. *Empirical Distributions and Exploratory Data Analysis*, in: Statistical Methods Atmospheric Science 4th Edition. Amsterdam: Elsevier Ltd; 2019: pp. 23–75. DOI: https://doi.org/10.1016/B978-0-12-815823-4.00003-1.

.